*MRS Communications (2023) 13:248–255*

https://doi.org/10.1557/s43579-023-00336-3

MRS Communications

Research Letter

# Humidity sensing performance of polyaniline-neodymium oxide composites

**L. B. Gunjal,** Department of Physics, VTU-RC, RYM Engineering College, Ballari 583104, India
**S. Manjunatha,** Department of Physics, V.V. Sangha's Independent PU College, Ballari 583104, India
**B. Chethan,** Department of Physics, Indian Institute of Science, Bengaluru, Bengaluru 560012, India
**N. M. Nagabhushana,** Department of Physics, VTU-RC, RYM Engineering College, Ballari 583104, India
**Y. T. Ravikiran,** Department of PG Studies & Research in Physics, Government Science College, Chitradurga 577501, India
**T. Machappa,** Department of Physics, VTU-RC, Ballari Institute of Technology & Management, Ballari 583104, India
**S. Thomas,** School of Energy Materials, Mahatma Gandhi University, Kottayam, Kerala, India 686560

Address all correspondence to N. M. Nagabhushana at **nagabhushananm@gmail.com** and Y. T. Ravikiran at **ytrcta@gmail.com**

(Received 26 October 2022; accepted 24 January 2023; published online: 13 February 2023)

## Abstract

Humidity sensing response of conducting polymer composite such as Polyaniline-Neodymium Oxide (PNO) composite with varying wt% of $Nd_2O_3$ in PANI [PANI-$Nd_2O_3$-10% (PNO-1), PANI-$Nd_2O_3$-30% (PNO-2) and PANI-$Nd_2O_3$-50% (PNO-3)] was studied. These samples were prepared by in situ chemical polymerization and were structurally and morphologically characterized by various analytical techniques. Humidity sensing performance of the PNO composites was evaluated in the range of 11–97% RH. Composite PNO-3 showed the highest sensing response of 99% with a response and recovery times of 28 and 29 s, respectively. Other sensing parameters like hysteresis, limit of detection, and sensing stability were also determined for the composites.

## Introduction

Humidity sensors have gained vital significance in the food production, food storage, medical field, agriculture, museums, libraries, electronic industry and nuclear power plants due to the increase in demand for their use in monitoring the controlled environments.[1] Recently, humidity sensors fabricated from materials such as metal oxides, ceramics, thin layers of aluminium oxide films have attracted considerable attention in the field of sensor research.[2] But most of these sensors have encountered many limitations, such as complex device fabrication, high operating temperature, high-power consumption, and high cost.[3] To overcome these disadvantages, conducting polymer-based humidity sensors have emerged as a competitive class of alternating material with a number of advantages, such as ease of fabrication, hygroscopicity and ambient temperature operability.[4] In addition, the sensing dependent electrical and related mechanical properties of the conducting polymers can be tuned in various ways; including doping, production of blends and composites, and use of various preparation procedures.[5]

Among all the conducting polymers, polyaniline (PANI) has emerged as an excellent polymer due to its chemical expediency and ease of synthesis along with the wide range of attractive applications in sensors, EMI shielding, corrosion protection, supercapacitors, etc.[6] PANI alone has exhibited very less sensitivity to humidity due to its less hygroscopicity. To fabricate efficient humidity sensors, PANI has been composited with diverse materials like metals, semiconductors, non-metals, metal oxides, and carbon materials such as fullerene, carbon nanotubes, graphene, graphene oxide.[7] To further enhance the scope of PANI based composites, in terms of water adsorption capacity, improved sensitivity, response, and recovery times, limit of detection and linearity, in the present work we have chosen PANI and composited with neodymium oxide ($Nd_2O_3$). Since it is a rare earth oxide with a hexagonal crystal system, which has a high dielectric constant and insolubility in water and favorable band offset with semiconductors, it finds applications in many microelectronic devices such as sensors.[8]

In this perspective, PNO composites with different wt% of $Nd_2O_3$ in polyaniline were synthesized by employing the in situ chemical polymerization, and then morphologically and structurally characterized by FESEM, TEM, XRD, FTIR and Raman studies before humidity sensing studies.

## Experimental

### *Materials*

Aniline ($C_6H_5NH_2$), Hydrochloric acid (HCl), Ammonium persulphate [$(NH_4)_2S_2O_8$], Neodymium oxide ($Nd_2O_3$) and de-ionized water all these analytical reagents (AR) grade chemicals were procured from SD fine chemicals, Mumbai, India.

L. B. Gunjal and S. Manjunatha have contributed equally to this work.

## Synthesis of PANI and PNO composites

PANI was prepared by in situ chemical polymerization technique. By adding 2 mL aniline with 0.1 mol $L^{-1}$ to 100 mL HCl (8.58 mL of 1 M HCl added in 100 mL distilled water) and continuously subjected to magnetic stirring for 6 h to get a homogeneous mixture. To the reactant mixture, ammonium persulphate of 0.1 mol $L^{-1}$ (2.28 g was dissolved in distilled water of 100 mL) was added to the mixture of reactants and left for polymerization. The product obtained after polymerization was separated and washed with 1N HCl and de-ionized water. Further, the dark-green product was kept in an oven for 24 h to obtain a dry powder. Under the similar conditions, PNO composites, namely PNO-1, PNO-2 and PNO-3 were prepared by adding crushed $Nd_2O_3$ powder of 10, 30 and 50 wt% with respect to PANI yield during the polymerization reaction respectively.

## Characterization

Pestled samples of PANI, $Nd_2O_3$ and PNO composites were used to record the X-ray diffraction (XRD) spectra in the $2\theta$ range 10–80° using D8 Advance Bruker X-ray diffractometer at a scan rate of 1.1° $min^{-1}$ with Cu-Kα radiation as X-ray source of wavelength $\lambda = 1.54$ Å. To record the Fourier-transform infrared (FTIR) spectra, KBr pellets of the synthesized samples were prepared first, under a hydraulic pressure of 4–5 tons, and then pellets were introduced in to Perkin Elmer spectrum 65 instrument at a resolution of 4 $cm^{-1}$. Field emission scanning electron microscopy (FESEM) was used to examine the surface morphology of the samples. FESEM images were obtained by Quanta 3D FEG and FEI Nova Nano SEM 600 instruments. JEOL-3010 instrument (fitted with a Gatan CCD camera) was used to capture the Transmission electron microscopy (TEM) image of PNO-3 composite. To capture TEM images, an accelerating voltage of 300 kV was applied. Raman studies were conducted using Horiba JobinYvon LabRam HR 800 spectrometer, employing Ar laser of power 20 mW and wavelength 514 nm in the wavenumber range 200 to 2000 $cm^{-1}$.

## Humidity sensing studies

An experiment to examine the ambient temperature humidity sensing characteristics was carried out by preparing pellets of PANI and the PNO composites with a thickness 1.5 mm and of diameter 10 mm applying a hydraulic press. Pellets were coated with silver on both sides to provide ohmic contacts. A hygrometer (Mextech-DT-615) was used to monitor the specific relative humidity, which was maintained in glass chambers by saturated solutions of various salts, viz. LiCl (11.3% RH), $K(CH_3COO)$ (22.7% RH), $MgCl_2$ (33.1% RH), $K_2CO_3$ (43.2% RH), $Mg(NO_3)_2$ (53.0% RH), $COCl_2$ (64.0% RH), NaCl (75.7% RH), KCl (85.1% RH), $K_2SO_4$ (97.6% RH). Electrodes were placed inside the glass chamber, which also holds the pellet through the rubber plugs fixed on the surface of the glass chambers. An Impedance analyzer (Hioki, Japan, Model: IM 7587) was connected to one end of the electrodes to measure impedance before and after exposure to a specific relative humidity. This meter was preferred to measure the change in impedance as a function of relative humidity for each sample at a chosen frequency of 100 Hz while maintaining a constant room temperature of 28°C in the RH range of 11 to 97%, avoiding polarization effects, if any. A particular frequency of 100 Hz was chosen, since these samples are known to exhibit the best linearity in impedance and a quick increase in capacitance over the tested RH range. The detailed description of humidity sensing measurements and the schematic diagram of experimental set up are given in our earlier papers.[9]

The formula to calculate the sensing response of the sample at ambient temperature is given by Eq. (1).

$$\mathrm{SR} = \left[\frac{Z_{\mathrm{LH}} - Z_{\mathrm{HH}}}{Z_{\mathrm{LH}}}\right] \times 100 \tag{1}$$

where SR—sensing response, $Z_{LH}$—impedance at lower % RH, $Z_{HH}$—impedance at various higher % RH. Further, the sensing performance of the composites has been evaluated by the method of least squares regression.[13] Then,

Limit of detection (LOD)[10] is computed using Eq. (2),

$$\mathrm{LOD} = 3.3 \times \left[\frac{\text{Standard deviation of the regression line}}{b}\right] \tag{2}$$

where $b$—slope of the least square fitted line, obtained by the graph impedance versus %RH, %Hysteresis in the humidity sensing behavior is calculated using Eq. (3)

$$\%\ \mathrm{Hysteresis} = \left[\frac{Z_{\mathrm{mn}} - Z_{mp}}{Z_{\max} - Z_{\min}}\right] \times 100 \tag{3}$$

where $Z_{mn}$ and $Z_{mp}$ are the maximum and minimum values of impedances at the mean value of %RH in the hysteresis humidity graph. $Z_{max}$ and $Z_{min}$ are the maximum and minimum values of measured impedances in the range 11–97% RH.

## Results and discussion

### *XRD studies*

Figure S1 shows the XRD patterns of PANI, $Nd_2O_3$ and PNO-3 composite with identified hkl values. XRD spectrum of PANI [Fig.S1(a)] has exhibited two major peaks at $2\theta = 21.32°$ and 25.49°, which corresponds to (100) and (111) planes respectively, and can be correlated to the periodicity of lattice, perpendicular and parallel to the polymer chains as per the literature.[9] Fig. S1(b) shows the XRD pattern of $Nd_2O_3$ for different values of $2\theta$, related to the crystal planes (110), (200), (211), (220), (310) and (321) respectively, which confirm its cubic crystal structure. The pattern matches well with the JCPDS file No. 83–1356.[11] XRD pattern of PNO-3 composite is shown in Fig. S1(c), has all the $Nd_2O_3$ peaks but with a reduced intensity, because $Nd_2O_3$ particles are embedded within the polymer matrix.

In addition, the XRD pattern of the composite (PNO-3) show that the distinctive peaks of $Nd_2O_3$ are retained with minor changes, whereas those of PANI have disappeared, showing that the crystalline structure of $Nd_2O_3$ in the composite remain unaffected.[12] Crystallite size of the composite computed using Debye–Scherrer formula was found to be 27.92 nm and that of $Nd_2O_3$ was 30.74 nm. As the crystallite size has reduced, increase in the surface to volume ratio, which may lead to the enhanced the water adsorption capacity in the composite. Another noteworthy finding is that the intense peak of $Nd_2O_3$ in the composite has shown suppressed intensity, implying that the presence of metal oxide in the composites might have enhanced surface active sites for water adsorption.[13]

## FTIR characterization

FTIR spectra of PANI, $Nd_2O_3$ and PNO-3 composite are depicted in Fig. S2. FTIR spectrum of PANI (Fig. S2(a)) reveals its characteristics absorption bands at 507, 862, 1150, 1307, 1488, 1582, 2320 and 3233 $cm^{-1}$.[14] The absorption band at 507 $cm^{-1}$ is due to the coupling of $Cl^-$ ions with bending vibrations of PANI.[15] Bands at 862, 1150 and 1307 $cm^{-1}$ correspond to C–H in plane stretching. Bands at 1488 $cm^{-1}$ represent C=C stretching in cyclic benzenoid and 1582 $cm^{-1}$ related to C=C stretching in the quinoid rings respectively. FTIR spectrum of $Nd_2O_3$ (Fig. S2(b)) shows its intense absorption band at 666 $cm^{-1}$, represent the characteristic stretching vibration of metal and oxygen (Nd-O).[15] The presence of bands of both $Nd_2O_3$ and PANI bands in the composites [Fig. S2(c)] indicates that the conjugated structure of PANI chains interacts with $Nd_2O_3$. Moreover, the existence of shifted bands of PANI and $Nd_2O_3$ in the composite spectrum with greater depth confirms their interfacial contact. And this contact could be due to the formation of hydrogen bonds between N–H of PANI and the oxygen of $Nd_2O_3$.

## FESEM and TEM studies

FESEM images of PANI, $Nd_2O_3$ and PNO-3 composite are depicted in Fig. 1. FESEM image of PANI shows clusters of agglomerated globular structures [Fig. 1(a)]. This kind of morphology is common in conducting polymers.[16] In the FESEM image of $Nd_2O_3$, uniformly distributed, densely packed clusters of grains can be observed [Fig. 1(b)]. FESEM image of PNO-3 composite [Fig. 1(c)] shows that, clusters of PANI granules deposited on $Nd_2O_3$ with pores. Such morphology readily facilitates water adsorption. Average grain size of the composite was calculated using image-J software by employing normal distribution [Fig. 1(d)]. Average grain size of the composite particles was found to be 0.35 μm, these grain clusters helpful for diffusion of water molecules through pores, which in turn enhances the humidity sensing performance of the composite.[12]

TEM image of PNO-3 composite is shown in Fig. 1(e). The image clearly illustrates how $Nd_2O_3$ particles are uniformly incorporated in to the PANI matrix.[17] Sizes of such composite particles were found to be in the range of 90–100 nm. SAED (selected area electron diffraction) pattern of the PNO-3 composite is shown in Fig. 1(f), which shows bright spots arising from Bragg reflection from a single crystallite, indicating the crystalline nature of the composite. Such crystalline composites helpful for fabrication of humidity sensors reported recently.[18]

## Raman studies

Raman spectra of PANI, Nd2O3 and PNDO-50% is shown in Fig. S3. Raman spectrum of PANI as in Fig. S3(a), exhibited its significant peaks at 1126, 1351 and 1577 $cm^{-1}$ which can be attributed to in-plane bending of C–H, stretching vibrations of C–N•+ and stretching vibrations in quinoid rings of C=C respectively. Raman spectrum of $Nd_2O_3$ is depicted in Fig. S3(b)has shown four phonon related bands of (2A2u+2Eu) at room temperature. Raman peaks of the oxide are found at 295, 352, 401, 466 $cm^{-1}$. Among these signature peaks of $Nd_2O_3$, the prominent peak can be seen at 352 $cm^{-1}$. Also, peak at 466 $cm^{-1}$, can be assigned to A2u mode. Apart from these peaks two shoulders can be seen at 568 and 773 $cm^{-1}$. Raman spectrum of the composite PNO-3, as in Fig. S3(c)exhibited the peaks of both PANI and $Nd_2O_3$, interestingly, the prominent peak 352 $cm^{-1}$ of $Nd_2O_3$, has been shifted to 325 $cm^{-1}$, indicating a strong interaction between PANI and $Nd_2O_3$. The peak shift towards the smaller wavenumber indicating the formation of the composite has exerted a tensile stress on the crystalline $Nd_2O_3$, which in turn has increased its bond length. This structural deformation in the crystalline composite has facilitated favorably for the water adsorption and there by contributing to the humidity sensing.[19]

## Humidity sensing studies

Variation in impedance of PANI and PNO composites in response to a vivid environment in the RH range 11–97% is depicted in Fig. S4. Impedance value decreases with increase in %RH for PANI and PNO composites as shown in Fig. S4. Decrease in the impedance of the composites with an increase in %RH exhibited a linear behavior, and therefore for the three composites, after applying the least square method, the value of linear correlation $R^2$ was calculated and tabulated (Table I) and the related plot is shown in Fig. 2(a). The point sensitivity, real sensitivity, limit of detection (LOD), and humidity hysteresis are the other sensing parameters computed using the Eqs. (1, 2 and 3) for PANI and the PNO composites and are listed in Table I.[9] Noteworthy observation from Table I, is that, for PNO-3 composite, point sensitivity of 91% at 97%RH, real sensitivity of 6.37 MΩ/% RH with a LOD of 4%RH, and the linearity $R^2$ of 0.998 have excelled over other composites. These favorable parameters of PNO-3 composite are deciding factors in the design of a competitive humidity sensor.

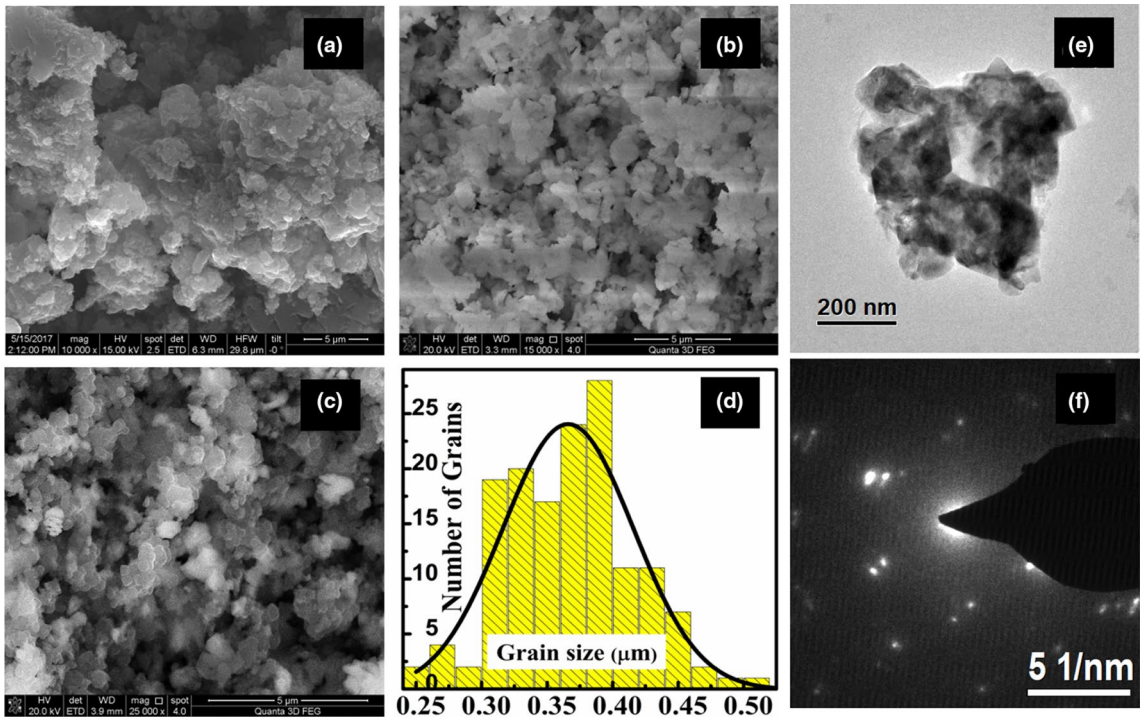


**Figure 1.** FESEM micrographs of (a) PANI, (b) $Nd_2O_3$ and (c) PNO-3 composite and (d) histograms of size distribution of the PNO-3 composite particles (e) TEM image of PNO-3 composite and (f) SAED pattern PNO-3 composite.

**Table I.** Point sensitivity, real sensitivity, limit of detection and linearity of PNO composites.

| Material | Point Sensitivity (%) (at 97%RH) | Real Sensitivity (MΩ/% RH) | Limit of detection (% RH) | Linearity ($R^2$) |
|---|---|---|---|---|
| PNO-1 | 77 | 2.81 | 19.4 | 0.972 |
| PNO-2 | 90 | 4.62 | 8.4 | 0.994 |
| PNO-3 | 91 | 6.37 | 4.0 | 0.998 |
| Timing behavior of various PANI composites | | | | |
| Hybrid material | Response time (s) | Recovery time (s) | Sensing range %RH | Reference |
| PANI/$Nd_2O_3$ | 28 | 29 | 11–97 | Present work |
| PANI/$SnO_2$ | 26 | 30 | 05–95 | [20] |
| PANI/$Ho_2O_3$ | 32 | 46 | 11–97 | [10] |
| PANI/$TaS_2$ | 36 | 49 | 11–97 | [14] |
| PANI/$WS_2$ | 56 | 70 | 10–97 | [21] |
| PANI/NiO | 60 | 90 | 5–90 | [22] |

## Timing behavior

Timing behavior is an important aspect in the design of any sensing material. Figure 2(b) shows the characteristic response and recovery curve of the PNO-3 composite. Response time and recovery time characteristics are very important parameters for evaluating the performance of any sensor. Initially, the sample was kept in a chamber containing 11% RH and then transferred to a chamber with a 97% RH, with a switching time of one second, which recorded a response time of 28 s. A recovery time of 29 s was recorded when the sample was brought back from the chamber with 97%RH to the 11%RH. The response and recovery times are almost same indicating that the exothermic and endothermic processes occur at the same rate.[23] Good response and recovery times of the composite may be due to the presence of smaller grain size as evidenced by the FESEM image. Therefore, this composite has best humidity sensing properties, making it a truly competent humidity

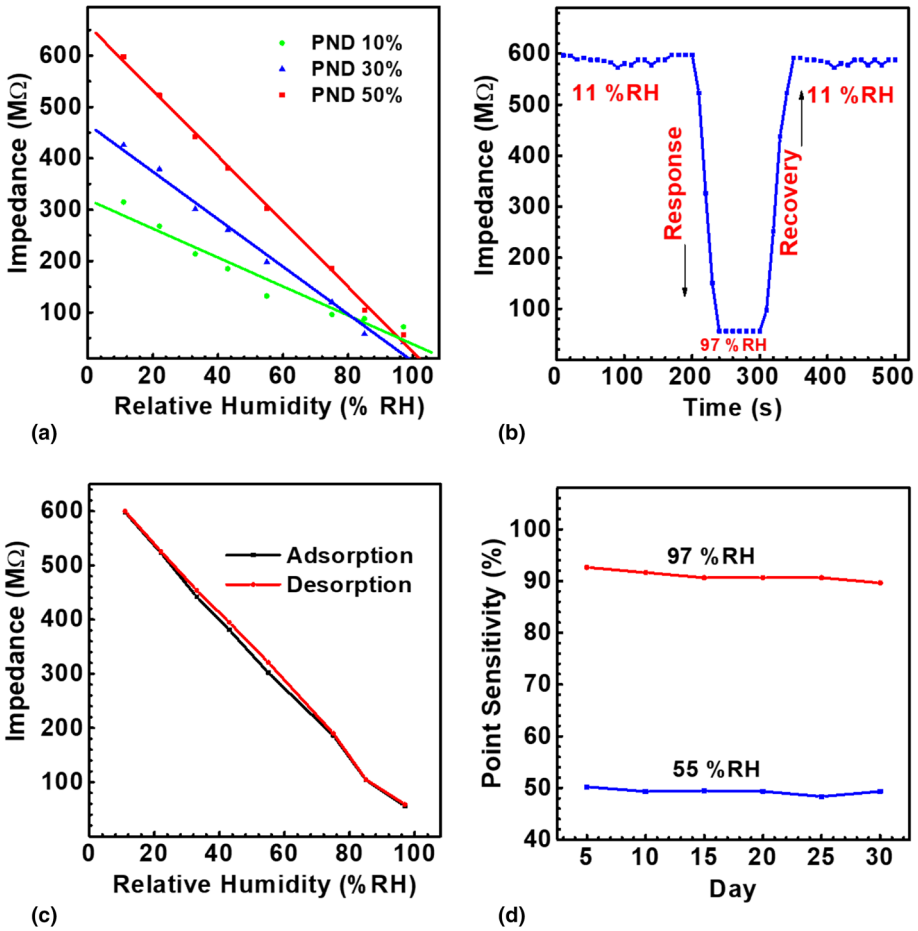


**Figure 2.** (a) Least square fits of the impedance of each composite for varied humid environments, (b) Response-recovery curves of PNO-3 composite, (c) Humidity hysteresis characteristic curves of PNO-3 composite, (d) Humidity sensing stability of PNO-3 composite.

sensing material. The response-recovery times for the various composites are listed in Table I.

## Humidity hysteresis and stability

Figure 2(c) shows the humidity hysteresis curve for PNO-3 composite. Impedance values were recorded by subjecting the composite sample at first in increasing and later in decreasing order of RH between 11 and 97%, the humidity hysteresis loss of PNO-3 composite was evaluated experimentally. In the ascending order of humid environment, as prevailed in different humidity chambers of the experimental set up, the adsorption of water molecules was detected with a simultaneous decrease in the impedance of the composite. This impedance change, exhibited a linear behavior with an increase in %RH. Whereas, during the descending order of %RH environments, it is interesting that the impedance variation with decreasing %RH, followed a slightly different path as shown in Fig. 2(c), which indicates a desorption process.[24] Also, at an optimum value of 55% RH, the maximum difference in humidification and dehumidification was observed. In this humid environment, hysteresis loss was calculated to be 2%.

Humidity sensing stability test for PNO-3 composite was performed once in every five days for one month as shown in Fig. 2(d). The observed sensing responses in two different relative humidity environments particularly at 55%RH and 97%RH were found to be nearly stable, implying that the composite acts as a stable humidity sensor.

## Humidity sensing mechanism

The three steps of the humidity sensing mechanism are chemisorption, physisorption and capillary condensation. At the lower RH level, chemical adsorption of water molecules occurs on active sites on the surface of the sensing material, which then dissociates into $H^+$ and $OH^-$ ions due to self-ionization.[25] When PNO-3 composite was exposed to ambient humidity, the water vapour self-ionizes to form proton $H^+$ and hydroxyl ions $OH^-$ as depicted in Eq. (4). Because metal cations have a high density of charge carriers with a strong electric field, these ions

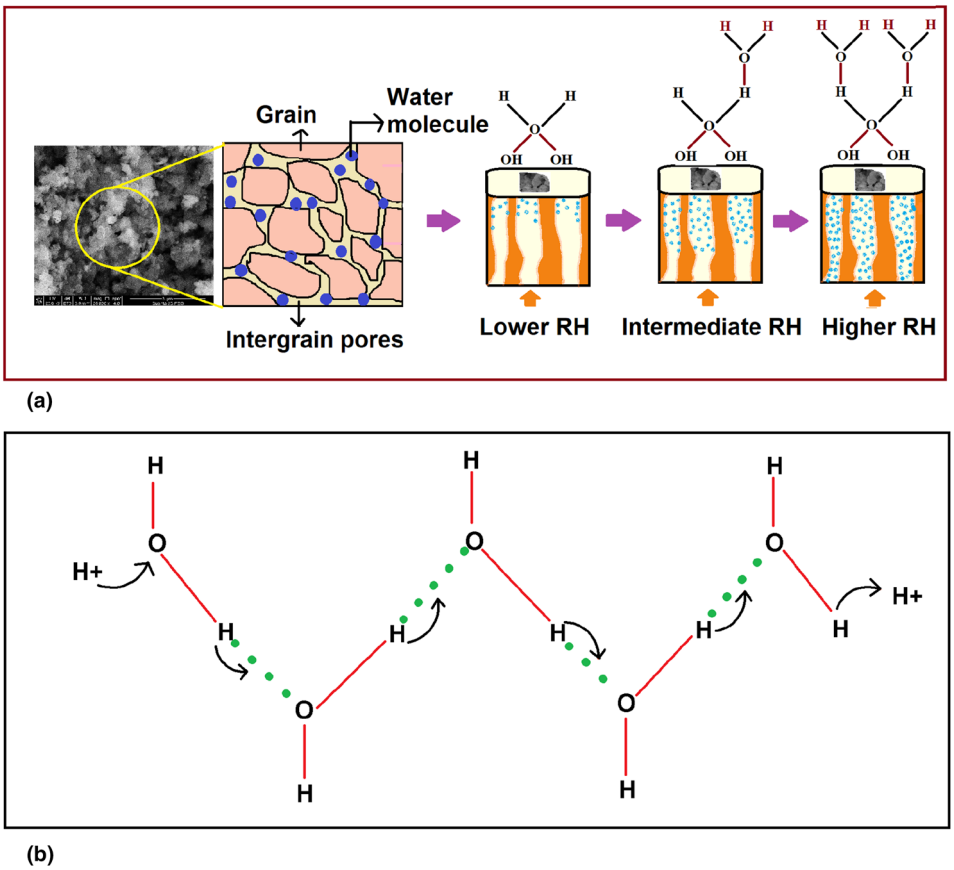


**Figure 3.** (a) Schematic diagram of sensing mechanism, (b) Grotthus reaction.

cause protonation and condensation on the surface of PNO-3 composite.

$$H^+ + OH^- \rightleftharpoons H_2O \quad (4)$$

With increase in the relative humidity, a chemisorbed layer of ions is formed due to the chemical adsorption of water vapour to the active sites of the composite surface. At the same time, the dissociated hydroxyl ions bind to the highly charged surfaces of the metal cations and the released $H^+$ ions flow freely on the surface of the composite, thereby slightly increasing its conductivity. As this process proceeds, with the increase in relative humidity, two $OH^-$ ions form hydrogen bonds with a water molecule, generating $H_3O^+$ and $OH^-$ ions, as shown in Eq. (5) and the resulting layer is known as a physisorbed layer and this layer becomes stationary due to hydrogen bonding.[26]

$$2H_2O \rightarrow H_3O^+ + OH^- \quad (5)$$

As %RH further increases, huge water molecules accumulate on the top of the already formed physisorbed layers. These physisorbed layers would pile up on the top of each other; creating an extremely unstable mass of $H_3O^+$. As a result, it rapidly splits into a water molecule and a proton, as shown in Eq. (6) and shown in Fig. 3(b). This process is called Grotthus reaction.[27]

$$H_3O^+ \rightarrow H_2O + H^+ \quad (6)$$

Later, when the humidity is extremely high, more water molecules are adsorbed on the surface of the composite, eventually leading to the formation of poly-physisorbed layers that release many protons. These charged particles migrate from one water molecule to another, simultaneously making and breaking bonds with nearby molecules, releasing a huge number of protons leading through various water molecules, resulting in a drastic reduction in impedance.[21] As a result, in a particularly humid environment, protons are the main charge carriers. At the end of the process water molecules begin to condense in the capillary pores formed due to the reduced grain size as evident from XRD, which lead to the electrolytic conduction, which in turn resulted in further decrease in impedance. Figure 3(a) depicts the predicted condensation mechanism.

Overall, the PNO-3 composite, exhibited a good sensitivity, fast timing behavior, minimal humidity hysteresis and good humidity sensing stability as compared to the PANI and other

composites at room temperature. All these features are worth considering, when designing a reliable humidity sensor.

## Conclusion

PANI composites using rare earth neodymium oxide were prepared by in situ chemical polymerization technique by changing the composition of the oxide in the PANI. Composites were investigated for their humidity sensing behavior. Of all the composite samples, PNO-3 composite prevailed with appreciable response, recovery times of 28 and 29 s, minimal humidity hysteresis, in addition to stability in sensing for a period of one month. From these obtained results, it follows that the PNO composite is an effective material in the fabrication of the humidity sensor that can be operated at the ambient temperature.

## Funding

No funding support received from any funding agencies.

## Declarations

### Competing interests

The authors declare that they have no competing interests.

## Ethical approval

This article does not contain any studies with human participants or animals performed by any of the authors.

## Supplementary Information

The online version contains supplementary material available at https://doi.org/10.1557/s43579-023-00336-3.

## References

1. B. Chethan, H.G. Raj Prakash, Y.T. Ravikiran, S.C. Vijaya Kumari, C.V.V. Ramana, S. Thomas, D. Kim, Enhancing humidity sensing performance of polyaniline/water soluble graphene oxide composite. Talanta **196**, 337–344 (2019)
2. D. Nunes, A. Pimentel, A. Gonçalves, S. Pereira, R. Branquinho, P. Barquinha, E. Fortunato, R. Martins, Metal oxide nanostructures for sensor applications. 2D Mater. **34**, 043001 (2019). https://doi.org/10.1088/2053-1583/abe778
3. F. Fang, J. Kennedy, J. Futter, T. Hopf, A. Markwitz, E. Manikandan, G. Henshaw, Size-controlled synthesis and gas sensing application of tungsten oxide nanostructures produced by arc discharge. Nanotechnology **22**, 335702 (2011). https://doi.org/10.1088/0957-4484/22/33/335702
4. C. Feng, S. Sun, H. Wang, C.U. Segre, J.R. Stetter, Humidity sensing properties of Nation and sol-gel derived $SiO_2$/Nation composite thin films. Sens. Actuators B Chem. **40**, 217–222 (1997). https://doi.org/10.1016/S0925-4005(97)80265-1
5. R. Megha, Y.T. Ravikiran, S.C.V. Kumari, H.G.R. Prakash, M. Revanasiddappa, S. Manjunatha, S.G. Dastager, S. Thomas, Structural and electrical characterization studies for ternary composite of polypyrrole. J. Mater. Sci. Mater. Electron. **31**, 18400–18411 (2020). https://doi.org/10.1007/s10854-020-04386-4
6. M. Beygisangchin, S.A. Rashid, S. Shafie, A.R. Sadrolhosseini, H.N. Lim, Preparations, properties, and applications of polyaniline and polyaniline thin films—a review. Polymers (Basel). **13**, 2003 (2021). https://doi.org/10.3390/polym13122003
7. V. Babel, B.L. Hiran, A review on polyaniline composites: synthesis, characterization, and applications. Polym. Compos. **42**, 3142–3157 (2021). https://doi.org/10.1002/pc.26048
8. V. Manikandan, A. Mirzaei, I. Petrila, S. Kavita, R.S. Mane, J.C. Denardin, S. Lundgaard, S. Juodkazis, J. Chandrasekaran, S. Vigneselvan, Effect of neodymium stimulation on the dielectric, magnetic and humidity sensing properties of iron oxide nanoparticles. Mater. Chem. Phys. **254**, 123572 (2020). https://doi.org/10.1016/j.matchemphys.2020.123572
9. B. Chethan, H.G.R. Prakash, Y.T. Ravikiran, S.C.V. Kumari, S. Manjunatha, S. Thomas, Humidity sensing performance of hybrid nanorods of polyaniline-Yttrium oxide composite prepared by mechanical mixing method. Talanta **215**, 120906 (2020). https://doi.org/10.1016/j.talanta.2020.120906
10. S. Manjunatha, T. Machappa, Y.T. Ravikiran, M. Chethan, M. Revanasiddappa, Room temperature humidity sensing performance of polyaniline – holmium oxide composite. Appl. Phys. A. **125**, 361 (2019). https://doi.org/10.1007/s00339-019-2638-1
11. P. Aldebert, J.P. Traverse, Study by neutron diffraction of the high temperature structures of $La_2O_3$ and $Nd_2O_3$. Mater. Res. Bull. **14**, 303–323 (1979). https://doi.org/10.1016/0025-5408(79)90095-3
12. R. Najjar, S. Nematdoust, A resistive-type humidity sensor based on polypyrrole and ZnO nanoparticles: hybrid polymers vis-a-vis nanocomposites. RSC Adv. **6**, 112129–112139 (2016). https://doi.org/10.1039/C6RA24002J
13. J. Shah, M. Arora, L.P. Purohit, R.K. Kotnala, Significant increase in humidity sensing characteristics of praseodymium doped magnesium ferrite. Sens. Actuators A Phys. **167**, 332–337 (2011). https://doi.org/10.1016/j.sna.2011.03.010
14. S. Manjunatha, T. Machappa, Y.T. Ravikiran, B. Chethan, A. Sunilkumar, Polyaniline based stable humidity sensor operable at room temperature. Phys. B Condens. Matter. **561**, 170–178 (2019). https://doi.org/10.1016/j.physb.2019.02.063
15. S. Manjunatha, A. Sunilkumar, Y.T. Ravikiran, T. Machappa, Effect of holmium oxide on impedance and dielectric behavior of polyaniline–holmium oxide composites. J. Mater. Sci. Mater. Electron. **30**, 10332–10341 (2019). https://doi.org/10.1007/s10854-019-01371-4
16. Y.T. Ravikiran, M.T. Lagare, M. Sairam, N.N. Mallikarjuna, B. Sreedhar, S. Manohar, A.G. MacDiarmid, T.M. Aminabhavi, Synthesis, characterization and low frequency AC conduction of polyaniline/niobium pentoxide composites. Synth. Met. **156**, 1139–1147 (2006). https://doi.org/10.1016/j.synthmet.2006.08.005
17. S. Manjunatha, T. Machappa, A. Sunilkumar, Y.T. Ravikiran, Tungsten disulfide: an efficient material in enhancement of AC conductivity and dielectric properties of polyaniline. J. Mater. Sci. Mater. Electron. **29**, 11581–11590 (2018). https://doi.org/10.1007/s10854-018-9255-1
18. A. Sunilkumar, S. Manjunatha, B. Chethan, Y.T. Ravikiran, T. Machappa, Polypyrrole–tantalum disulfide composite: an efficient material for fabrication of room temperature operable humidity sensor. Sens. Actuators A Phys. (2019). https://doi.org/10.1016/j.sna.2019.111593
19. M.R. Joya, J.E. Alfonso, L.C. Moreno, Photoluminescence and Raman studies of $\alpha$- $MoO_3$ doped with erbium and neodymium. Curr. Sci. **116**, 1690–1695 (2019). https://doi.org/10.18520/cs/v116/i10/1690-1695
20. S.K. Shukla, S.K. Shukla, P.P. Govender, E.S. Agorku, A resistive type humidity sensor based on crystalline tin oxide nanoparticles encapsulated in polyaniline matrix. Microchim. Acta. **183**, 573–580 (2016). https://doi.org/10.1007/s00604-015-1678-2
21. S. Manjunatha, B. Chethan, Y.T. Ravikiran, T. Machappa, Room temperature humidity sensor based on polyaniline- tungsten disulfide composite. AIP Conf. Proc. **1953**, 030096-1-030096–4 (2018). https://doi.org/10.1063/1.5032431
22. P. Singh, C.S. Kushwaha, S.K. Shukla, G.C. Dubey, P. Singh, C.S. Kushwaha, S.K. Shukla, G.C. Dubey, Synthesis and humidity sensing properties of NiO intercalated polyaniline nanocomposite. Polym. Plast.

Technol. Eng. **58**, 139–147 (2019). https://doi.org/10.1080/03602559.2018.1466170
23. K.P. Biju, M.K. Jain, Effect of polyethylene glycol additive in sol on the humidity sensing properties of a $TiO_2$ thin film. Meas. Sci. Technol. **18**, 2991–2996 (2007). https://doi.org/10.1088/0957-0233/18/9/033
24. V.R. Khadse, S. Thakur, K.R. Patil, P. Patil, Humidity-sensing studies of cerium oxide nanoparticles synthesized by non-isothermal precipitation. Sens. Actuators B Chem. **203**, 229–238 (2014). https://doi.org/10.1016/j.snb.2014.06.107
25. B. Chethan, H.G.R. Prakash, Y.T. Ravikiran, S.C. Vijayakumari, S. Thomas, Polypyyrole based core-shell structured composite based humidity sensor operable at room temperature. Sens. Actuators B Chem. **296**, 126639 (2019). https://doi.org/10.1016/j.snb.2019.126639
26. B. Chethan, Y.T. Ravikiran, S.C. Vijayakumari, H.G. Rajprakash, S. Thomas, Nickel substituted cadmium ferrite as room temperature operable humidity sensor. Sens. Actuators A Phys. **280**, 466–474 (2018). https://doi.org/10.1016/j.sna.2018.08.017
27. F.M. Ernsberger, Nonconformist Ion. J. Am. Ceram. Soc. **66**, 747–750 (1983)